Mathematical Modelling, Vol. 7, pp. 1045–1069, 1986

0270–0255/86 $3.00 + .00

NETWORK COMPUTER ANALYSIS OF THE HUMAN KIDNEY†

RICHARD J. ROMAN*

Department of Physiology
Medical College of Wisconsin
Milwaukee, WI 53226, USA

and

FRED R. SIAS, JR.‡

Department of Electrical and Computer Engineering
Clemson University
Clemson, SC 29634-0915, USA

(*Received* 5 *February* 1985; *revised* 15 *July* 1985)

Abstract—A computer model of the human nephron is presented that predicts urine flow, sodium and potassium excretion, urine osmolality, etc., as well as pressures, flows and solute concentrations throughout the nephron as a function of arterial pressure, neural and hormonal inputs to the kidney and the concentrations of various solutes in the medullary interstitium. The model includes a feedback control system for regulating glomerular filtration rate and equations that equate model parameters to plasma levels of renal hormones. By modifying any of 49 parameters in an interactive control section of the program, the effects of complex abnormalities in hormonal control of the kidney and/or various renal diseases can be studied. Moreover, the model appears useful in evaluating hypotheses concerning the mechanism(s) of such complex phenomena as pressure diuresis, glomerular-tubular balance, the role of the kidney in hypertension and the influence of aging on renal function.

1. INTRODUCTION

The interplay of physical, neural, circulating hormonal and intrarenal humoral factors which regulate the function of the kidney makes it difficult to assess the overall effect of a disease or a therapeutic intervention on the excretion of sodium and water. It is very challenging, for example, to predict the change in sodium excretion when two opposing hormone systems are altered simultaneously. These questions concerning the response of the kidney to perturbations in complex control systems are ideally suited to computer analysis of a mathematical model.

Over the last 40 years numerous models have been developed to better our understanding of kidney function. The renal concentrating mechanism[1–4], the vasa recta countercurrent exchange process[5, 6] and the coupling of fluid and water reabsorption in the proximal tubule[6–9] have received particular attention. There have been fewer attempts at modeling whole kidney function[10–13] and none of these previous models have considered the interactions of the kidney with the rest of the cardiovascular system. The difficulties in developing a whole kidney model has been discussed in detail by Jacquez

† Computer diskette available.

* Send correspondence to Dr. Richard J. Roman, Department of Physiology, Medical College of Wisconsin, 8701 Watertown Plank Road, Milwaukee, WI 53226, USA.

‡ Send reprint requests and requests for copies of the computer program to Dr. Fred R. Sias, Jr., Dept. of Electrical and Computer Engineering, Clemson University, Clemson, SC 29634-0915, USA

and Carnahan[10]. Although they were successful in deriving a set of nonlinear partial differential equations that described kidney function, they were unable to solve these equations using existing mathematical or computer methods.

In the present study, we have developed a computer model of the human kidney that predicts 56 variables, such as urine flow, urine osmolality, sodium excretion, etc., as well as flows and pressures throughout the nephron, as a function of arterial pressure and levels of neural and hormonal inputs to the kidney. The model is written in Fortran and is sufficiently compact to run on personal microcomputers with 256K of memory. The model includes an interactive control section which allows the user to alter any or all of 49 parameters such as hormone levels, hydraulic resistances, tubular water permeabilities and solute transport rates throughout the nephron. Through manipulation of the parameters, the effects of abnormalities in hormonal control or the effects of renal disease on kidney function can be studied. Moreover, various hypotheses concerning the mechanisms underlying such complex phenomena as pressure diuresis, glomerular tubular balance or the effects of aging on renal function can be evaluated.

2. MODEL DESCRIPTION

A mathematical model of the kidney may be based on a distributed or compartmentalized view of the nephron. Most previous investigators have attempted to develop distributed models over a limited region of the nephron[1–9]. Jacquez and Carnahan[10] have described a complex set of partial differential equations which represent a distributed model of the entire renal cortex; however, these equations could not be solved analytically and have yet to be solved using a computer. Some of the problems in solving large distributed renal models revolve around difficulties in defining boundary conditions for solute concentration in the interstitium. Additionally, many important parameters such as tubular compliances, capillary reflection coefficients and the volumes of intracellular and intercellular compartments have not as yet been measured.

Consequently, to obtain a solvable whole kidney model we based our analysis on a compartmental model of a single nephron. We have limited the analysis to the steady state so that the system may be represented by a set of simultaneous algebraic rather than differential equations. In the steady-state solution, poorly defined constants such as tubular and capillary compliances and single nephron vascular and interstitial volumes become irrelevant. A steady-state solution is also consistent with the goal of describing kidney function as it interacts with the rest of the cardiovascular system over periods of hours and days since transients in renal function are usually brief and reach steady-state values within a few minutes. Finally, the compartmental modeling approach that was used best fits the experimental methods used to define single nephron transport parameters on which the model was based. Micropuncture determinations of tubular transport of solute and measurements of tubular water and solute permeabilities represent average measurements made between two tubular puncture sites. They provide no information of how the rate of transport changes with distance along the tubular segment studied.

The model of the human nephron described herein incorporates the anatomical features depicted in Fig. 1. It includes a glomerulus and a proximal tubule, thick ascending loop of Henle, and a distal tubule-cortical collecting duct segment that interacts with a cortical interstitium and a peritubular capillary compartment. The cortical interstitium was assumed to be a single well-mixed compartment with a composition identical to that of systemic plasma. Fluid exiting the cortical collecting duct drains into a medullary collecting duct that interacts with a series of medullary interstitium-vasa recta capillary compartments. The medullary interstitium and vasa recta compartments were also assumed

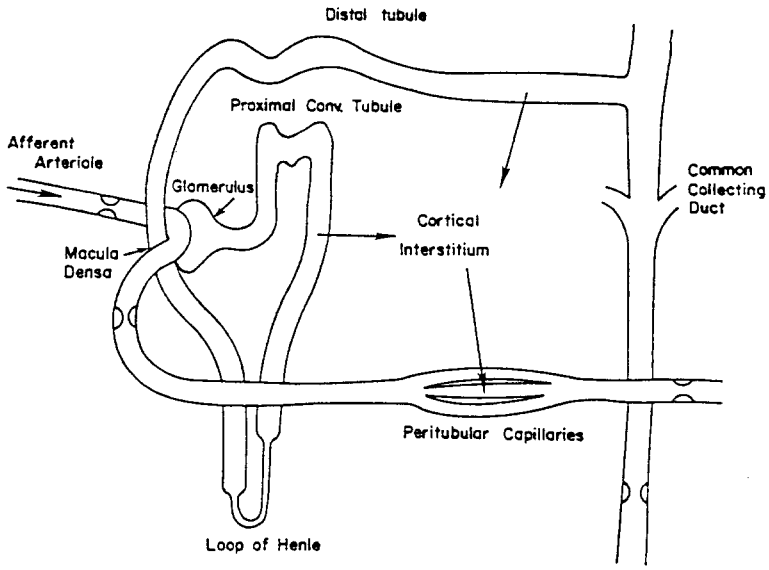

Fig. 1. Schematic representation of a simplified human nephron. Fluid reabsorbed from the proximal tubule, thick ascending limb and cortical collecting duct enters the cortical iterstitial compartment. Fluid exiting the cortical collecting duct enters the medullary collecting duct. Fluid reabsored from the medullary collecting duct is taken up into the medullary interstitial-vasa recta compartments. Fluid exiting the medullary collecting duct is excreted as urine.

to be well mixed. The urea and sodium chloride concentrations within the medullary interstitial compartments were included as parameters of the model.

The equivalent electrical circuit diagram of the model of the nephron is presented in Fig. 2. Hydraulic, oncotic or osmotic forces for fluid reabsorption are represented as variable batteries and labeled as P terms. R terms represent hydraulic resistances to fluid flow. K terms represent ultrafiltration coefficients. Arterial pressure drives renal blood flow, F_1, into the glomerulus at node 1 in Fig. 2. Some fluid, F_2, is filtered and is reabsorbed from the proximal tubule at node 5 into the interstitium (node 7) and back into the peritubular capillary compartment (node 2). The remaining fluid, F_3, flows through the loop of Henle and enters the cortical collecting duct compartment at node 6. A portion of this fluid is reabsorbed into the cortical peritubular capillaries (node 2) and the remainder, F_4, enters the medullary portion of the model at node 8. A portion of the fluid entering the medullary collecting duct F_4 is reabsorbed into the medullary interstitium at nodes 8–11. Fluid which is not reabsorbed in the medulla is excreted as urine at node 3. The fluid reabsorbed into the medullary interstitium returns via the vasa recta to the systemic circulation at node 14.

The hydraulic network depicted in Fig. 2 can be represented by eight simultaneous algebraic equations based on Kirchoff's law. Loop equations were written for the eight flows F_1–F_8 in each of the closed pathways indicated in Fig. 2. According to Kirchoff's law, the sum of the pressure drops (flow times resistance terms) and the pressure rises (hydraulic forcing functions) in any closed loop must equal zero. For example, consider the loop connecting nodes 1–4 and the flows contained in that loop, F_1, F_2 and F_4. Around this loop the pressure rise due to arterial pressure, PART, equals the pressure drops across RAFF, REFF and RVEN; i.e. F_1 times the sum of these resistances. Flows F_2 and F_4 oppose F_1 through common hydraulic elements REFF and RVEN. The pressure drop resulting from F_2 is equal to $F_2 \times$ REFF and that from F_4 equals $F_4 \times$ RVEN. The overall

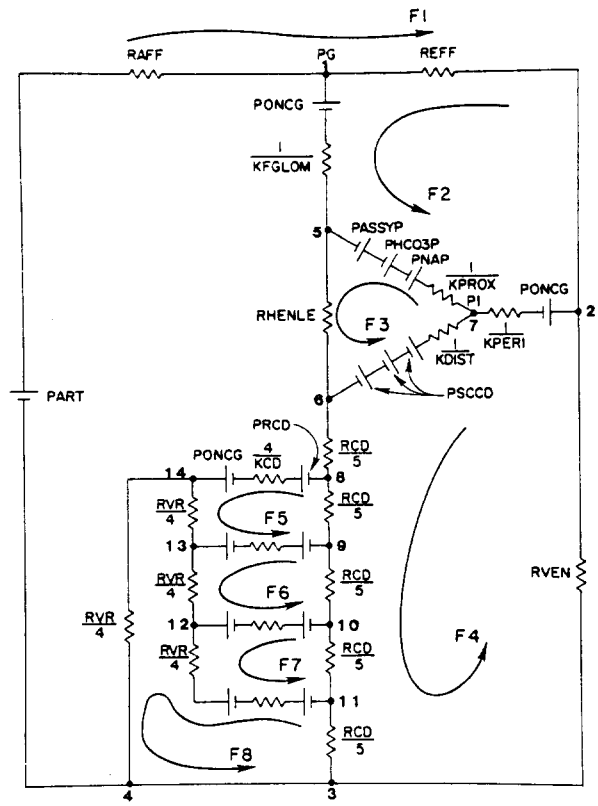

Fig. 2. Equivalent electrical circuit diagram of a human nephron.

equation for the loop connecting nodes 1–4 is defined in Eq. (1) below. Seven additional independent loop-flow equations were derived similarly and are described below in Eqs. (2)–(8). These eight simultaneous algebraic equations were easily solved using computer matrix methods.

$$\text{PART} = F_1 \times (\text{RAFF} + \text{REFF} + \text{RVEN}) - F_2 \times (\text{REFF}) - F_4 \times (\text{RVEN}), \quad (1)$$

$$\text{PASSYP} + \text{PHCO3P} + \text{PNAP} = -F_1 + F_2 \times (\text{REFF} + 1/\text{KFGLOM} + 1/\text{KPROX} + 1/\text{KPERI}) - F_3 \times (1/\text{KPROX}) - F_4 \times (1/\text{KPROX}), \quad (2)$$

$$\text{PSCCD} - \text{PASSYP} - \text{PHCO3P} - \text{PNAP} = -F_2 \times (1/\text{KPROX}) + F_3 \times (1/\text{KPROX} + 1/\text{KDIST} + \text{RHENLE}) - F_4 \times (1/\text{KDIST}), \quad (3)$$

$$\text{PSCCD} + \text{PONCG} = -F_1 \times (\text{RVEN}) - F_2 \times (1/\text{KPERI}) - F_3 \times (1/\text{KDIST}) + F_4 \times (\text{RVEN} + \text{RCD} + 1/\text{KDIST} + 1/\text{KPERI}), \quad (4)$$

$$\text{PCDIN} + \text{PRCD}(1) - \text{PRCD}(2) = F_5 \times (\text{RVR}/4 + 8/\text{KCD} + \text{RCD}/5) - F_6 \times (4/\text{KCD}) - F_8 \times (\text{RVR}/4), \quad (5)$$

$$\text{PCDIN} + \text{PRCD}(2) - \text{PRCD}(3) = -F_5 \times (4/\text{KCD}) + F_6 \times (\text{RVR}/4 + 8/\text{KCD} + \text{RCD}/5) - F_7 \times (4/\text{KCD}) - F_8 \times (\text{RVR}/4), \quad (6)$$

$$\text{PCDIN} + \text{PRCD(3)} - \text{PRCD(4)} = -F_6 \times (4/\text{KCD}) + F_7 \times (\text{RVR}/4 + 8/\text{KCD} + \text{RCD}/5) - F_8 \times (4/\text{KCD} + \text{RVR}/4), \quad (7)$$

$$\text{PCDIN} + \text{PRCD(4)} + \text{PONCG} = -F_5 \times (\text{RVR}/4) - F_6 \times (\text{RVR}/4) - F_7 \times (\text{RVR}/4 + 4/\text{KCD}) + F_8 \times (\text{RVR} + 4/\text{KCD} + \text{RCD}/5). \quad (8)$$

Parameters

Normal values for all the parameters used in the model are presented in Table 1. The filtration coefficients (K terms) were derived from reported hydraulic conductivities measured in rats or rabbits[14, 15], since data on the water permeabilitity of various nephron

Table 1

**** HUMAN MODEL PARAMETER ASSIGNMENTS ****

A1 :	2.08000		Coefficient for calculating COP
B1 :	.04800		Coefficient for calculating COP
CPROTA:	6.50000	g/dl	Arterial protein concentration
CO2A :	40.00000	mmHg	Arterial Partial pressure of CO2
CKA :	4.00000	mEq/l	Arterial Potassium concentration
FHI :	18.50000	nl/min	Initial flow in loop of Henle
GAIN :	5.00000		Factor in tubular-glomerular feedback
HALDO :	8.00000	ng/dl	Aldosterone conc. in plasma
HADH :	3.00000	pg/ml	ADH concentration in plasma
HPRA :	2.00000	ngAI/ml/3hr	Plasma renin activity
NENA :	1.00000	x normal	Renal nerve activity
NEFNO :	2.40000	million	Total number of nephrons
HCT :	.45000	%	Arterial Hematocrit
KFGLOM:	3.80000	mmHg/nl/min	Glomerular Filtration Coeff.
KPROX :	.08739	mmHg/nl/min	Filtration Coef. prox. tubule
KPERI :	24.00000	mmHg/nl/min	Filtration Coef. peritubule capill.
KCD :	.00040	mmHg/nl/min	Filtration Coef. collecting ducts
KDIST :	.00530	mmHg/nl/min	Filtration Coef. distal tubules
PART :	100.00000	mmHg	Mean arterial pressure
PVEN :	.00000	mmHg	Venous pressure, assumed zero
PHART :	7.40000		Arterial pH
RAFF :	.10000	nl/min/mmHg	Resistance afferent arteriole
REFF :	.07000	nl/min/mmHg	Resistance efferent arteriole
RVEN :	.05300	nl/min/mmHg	Venous resistance, post peritubules
RCD :	2.00000	nl/min/mmHg	Resistance of cortical collecting duct
RMCD :	2.00000	nl/min/mmHg	Resistance of medullary collecting duct
RVR :	.10000	nl/min/mmHg	Resistance of vasa recta
RHENLE:	.50000	nl/min/mmHg	Resistance of loop of Henle
RAMAX :	.50000	nl/min/mmHg	Max. resistance constricted aff. arteriole
RAMIN :	.05000	nl/min/mmHg	Min. resistance of dialated aff. arteriole
TNAP :	85.00000	pmol/min/mm	Na transport rate in proximal tubule
TNAH :	1000.00000	pmol/min/mm	Na transport rate in loop of Henle
TNACCD:	4.33000	pmol/min/mm	Na transport rate in cort. coll. duct
TNAMCD:	34.20000	pmol/min/mm	Na transport rate in medullary coll. duct
THCO3P:	400.00000	pmol/min/mm	Bicarb. transport rate in prox. tubule
CSA :	300.00000	mEq/l	Arterial salt concentration
CUA :	3.00000	mmol/l	Arterial urea concentration
SSCD :	.90000		Reflect. coef. salt in collecting duct
SUCD :	.50000		Reflect. coef. urea in collecting duct
SHCO3 :	.96000		Reflect. coef. bicarb. in prox. tubule
SCL :	.50000		Reflect. coef. chloride in prox. tubule
DSCD :	.00001	nl/min	Diffusion coef. to salt in coll. duct
DELSCD:	25.00000	mEq/l	Salt gradient in collecting duct
DELSI :	48.00000	mEq/l	Salt gradient in med. interstitium
DELUCD:	50.00000	mmol/l	Urea gradient in collecting duct
DELUI :	120.00000	mmol/l	Urea gradient in med. interstitium
DUCD :	.00005	nl/min	Diffusion coef. to urea in coll. duct
DUL :	.06000	nl/min	Diffusion coef. to urea in Loop of Henle
SLPT :	.45000	min/nl	Slope of compliance of proximal tubule
YIPT :	14.60000	min/nl	Y-intercept of prox. tubule compliance curve
AGE :	25.00000	years	AGE

segments in the human does not exist. These reported hydraulic conductivities (P_f) for different portions of the nephron are given in Table 2. Since these reported P_f values were factored per cm^2 of surface area of the rabbit tubule, they had to be scaled for the human nephron by multiplying the value by the surface area of the tubular segment in the human. The surface areas of various tubular segments in the human were calculated from published data on the diameters and lengths of dissected human nephrons[11, 16]. The rationale for applying hydraulic conductivity data from the rabbit and rat to the human kidney is justified considering the similarity of nephron structure in these mammalian species. The nephron of all three species have similar features differing only in the length and diameter of each tubular segment[11, 16, 17].

All the forces for fluid movement in the model were represented as equivalent hydraulic pressures. These pressures were either hydrostatic or osmotic forces that sum algebraically across the tubular membrane to drive fluid reabsorption.

The osmotic forces were calculated from the difference in the solute concentrations across each tubular segment. The concentration of solutes in the tubular fluid was calculated by the model as described below. In addition to the osmotic forces for fluid reabsorption in renal tubules, an equivalent force for fluid movement secondary to active reabsorption of solute in each tubular segment of the nephron was calculated from reported tubular transport rates of various solutes as discussed below. The urea and ionic composition of blood in the peritubular capillaries of the renal cortex were assumed to equal that of systemic blood. Normal values for the concentration of these substances in blood are presented in Table 1 and were taken from data of Koushanpour *et al.*[11]. As discussed earlier, numerous models have been developed to explain the high concentrations of urea and sodium in the medullary interstitium. Nevertheless, the mechanisms responsible for the generation of the cortical medullary osmotic gradient remains an area of considerable controversy[18]. Instead of trying to predict the solute concentrations in the medulla, the concentration of urea and salt (primarily sodium chloride) in the interstitium at various levels of the medulla was considered as parameters of the model. Normal values for the urea and sodium concentration at various levels of the medulla are presented in Table 1 and were taken from the dog data of Schmidt-Nielsen and Robinson[19]. Data from the dog was used to model the human kidney, since the structure of the medulla and urinary concentrating ability are similar in man and dog.

Table 2

nephron segment	length (cm)	diameter (μm)	area (cm^2)	P_f hydraulic Conductance (cm^3/cm^2 · sec)	L_p[1] water Permeability (nl/cm^2 · min · mmHg)	$K=L_pA$ filtration coefficient (nl/min · mmHg)	k values used in model (nl/min · mmHg)
Proximal tubule	1.5 (11,16)	30 (11)	.0141	.035- .51 (14,15)	2-30	.028- .42	.087
Thick ascending loop of Henle	1.0 (16)	20 (11)	.0063	.0012 (14)	.070	.0004	0
Cortical Collecting duct	1.0 (11,16)	25 (4,16,17)	.0078	.0006- .037 (14) +ADH	.035- 2.2	.0003- .017	.001- .007
Medullary Collecting duct	1.5 (11,16)	35 (4,16,17)	.0165	? - .0067 (14) +ADH	? - .39	? - .0064	.0001- .0008

Numbers in parentheses indicate references from which values were obtained.

[1] $L_p = P_f \times (V_m/RT)$: where, V_m is the molar volume of water (cm^3/mole), R is the gas constant (cm^3 · atm/mole · °k), and T is temperature in °k. The value of L_p was converted to the units presented by multiplying by 760 mmHg-sec/60 atm-min.

Proximal tubule

The forces for fluid reabsorption in the proximal tubule were calculated by assuming fluid reabsorption is coupled to solute movement iso-osmotically. Under these conditions, fluid flux (Jv) can be defined using Eq. (9), where Js is solute flux, and Posm is plasma osmolality.

$$Jv = Js/\text{Posm}. \tag{9}$$

Jv is also defined by Eq. (10) below:

$$Jv = \text{KPROX} \times \text{Pequiv}. \tag{10}$$

where KPROX is the filtration coefficient of proximal tubule and Pequiv equals the effective hydrostatic force for fluid reabsorption. Rearranging terms, Pequiv can be calculated using Eq. (11):

$$\text{Pequiv} = Js/(\text{Posm} \times \text{KPROX}). \tag{11}$$

In the proximal tubule, we calculated driving forces for fluid reabsorption due to active reabsorption of sodium bicarbonate via a Na–H exchange process and for fluid reabsorption due to electrical neutral active reabsorption of sodium chloride according to Eqs. (12) and (13):

$$\text{PHCO3} = \text{THCO3P} \times \text{LT}/(\text{Posm} \times \text{KPROX}). \tag{12}$$

$$\text{PNAP} = \text{TNAP} \times \text{LT}/(\text{Posm} \times \text{KPROX}). \tag{13}$$

The value for THCO3P (Table 1) was taken from the proximal tubular transport rate for sodium bicarbonate measured in the dog by Wong and Quamme[20]. TNAP represents the active reabsorption of sodium chloride via an electrical neutral pathway expressed in pmol/min/mm length of tubule, and LT is the length of the proximal tubule expressed in mm. The value of TNaP (Table 1) was assumed to be 25% of THCO3P in accord with data of Warner and Lechene[21] and Green and Giebisch[22], indicating that active transport of sodium chloride accounts for about a fourth of the sodium and fluid reabsorption in the proximal tubule.

A passive force for water reabsorption in the proximal tubule was also included in the model. This force, PASSYP, is caused by the asymmetric distribution of chloride and bicarbonate ions that develops across the proximal tubule due to the preferential reabsorption of sodium bicarbonate in the early portions of the tubule. The magnitude of PASSYP was calculated using Eq. (14) as was originally described by Warner and Lechene[21]:

$$\text{PASSYP} = \text{RT} \times (\Delta\text{HCO3} \times \text{SHCO3} - \Delta\text{CL} \times \text{SCL}). \tag{14}$$

R represents the gas constant. T represents temperature, SHCO3 and SCL are proximal tubular reflection coefficients for sodium bicarbonate and sodium chloride, respectively, and HCO3 and CL are the lumen to blood concentration differences for bicarbonate and chloride across the proximal tubule expressed in mEq/l. Values for SHCO3 and SCL (Table 1) were taken from the work of Warner and Lechene[21]. Since bicarbonate reabsorption and the generation of the chloride-bicarbonate transtubular concentration gradients are distributed with length along the proximal tubule, PASSYP, PNAP and PHCO3P

were calculated with respect to distance along the proximal tubule using an iterative approach. An average values for these forces were then used in loop flow equation (2).

Loop of Henle

In short loops of Henle which predominate in the human kidney, the thick ascending limb of Henle is nearly impermeable to water[14]. There is only a short region of the loop in the thin descending limb of Henle where water reabsorption can occur[18]. The major transport functions which occur in the loop of Henle are active reabsorption of sodium chloride and passive secretion of urea[14, 18]. In order to simplify the present model of the nephron, we assumed that fluid is not reabsorbed in the loop of Henle. Therefore, the loop of Henle could be represented in the model (Fig. 2) simply as a hydraulic resistance between proximal and distal tubules. Active reabsorption of sodium chloride in the thick ascending limb of Henle is known to be load dependent[15]. That is more sodium and chloride is reabsorbed when distal delivery of sodium is increased[14, 15, 18, 23]. To simulate this behavior, we assumed that active reabsorption of sodium and chloride in the thick ascending loop of Henle obeys Michaelis–Menten kinetics and can be described by Eq. (15) below:

$$\text{LANACL} = \int_0^L \text{TNAH}/(1 + \text{CNACL}/\text{Km})\, dx. \tag{15}$$

where LANACL is the amount of sodium chloride reabsorbed in the loop of Henle, L is the length of the loop segment (10 mm), TNAH is the maximum rate of sodium transport in the thick ascending loop of Henle expressed in pmole/min/mm length of tubule, CNACL represents the sodium concentration of the luminal fluid, and Km is the affinity constant of the active transport system for sodium or chloride.

Since we assumed that no fluid was reabsorbed in the loop, the concentration of sodium at any point along the thick ascending limb was calculated as follows:

$$\text{CNACLL} = \text{CNAS} - \text{LANACL}/F_3, \tag{16}$$

where CNAS is the concentration of sodium in the proximal tubule and systemic circulation, LANACL is the net transport of sodium chloride up to that point in the loop and F_3 represents loop of Henle flow rate.

The net amount of urea secreted in the loop of Henle (U) was calculated according to Eq. (17):

$$U = \int_0^L \text{DUL} \times (\text{CUI2} - \text{CURL})\, dx. \tag{17}$$

The concentration of urea at any point along the loop was calculated using Eq. (18) below:

$$\text{CURL} = \text{CUA} + U/F_3. \tag{18}$$

where DUL is the diffusion coefficient for urea in the loop of Henle, CUI2 is the urea concentration in the medullary interstitium at level 2, CURL is the urea concentration in the lumen of the thick ascending limb and F_3 is the flow rate in the loop of Henle. The urea concentration in the second medullary level was used to represent the behavior of the "average loop of Henle," since the loop of Henle of some juxtamedullary nephrons

extend deep in the medulla, whereas the loops of superficial nephrons (which predominate in the human) usually do not enter the inner medullary interstitium[18, 23].

Cortical collecting duct

Transport in the distal convoluted tubule, connecting tubule and cortical collecting duct was lumped into a single compartment termed the distal tubule-cortical collecting duct segment (Fig. 2). The force for fluid reabsorption in this segment was calculated as follows:

$$\text{PSCCD} = RT \times [\text{POSMS} - (\text{CINCCD} + \text{CSCCD}/2)], \quad (19)$$

where R is the gas constant, T is temperature, POSMS is systemic plasma osmolality, CINCCD represents the osmolality of the fluid entering the cortical collecting duct and CSCCD is the osmolality of the fluid leaving the cortical collecting duct. Along the cortical collecting duct, we assumed that reabsorption of sodium chloride is accompanied by an equal and opposite secretion of potassium chloride[14, 15]. The rate of this exchange process was assumed to be regulated by plasma levels of aldosterone. The osmolality of the fluid leaving the cortical collecting duct (CSCCD) was calculated using Eq. (20):

$$\text{CSCCD} = F_3 \times \text{CINCCD}/F_4, \quad (20)$$

where F_3 is loop of Henle flow rate, CINCCD is osmotic concentration of the fluid entering the collecting duct and F_4 is flow rate leaving the cortical collecting duct.

The concentration of the individual solutes, *ie*, potassium (CKCCD), urea (CUCCD) and sodium (CNACCD), exiting the cortical collecting duct were calculated from Eqs. (21)–(23):

$$\text{CKCCD} = (F_3 \times \text{CKA} + \text{TNACCD} \times \text{LT})/F_4, \quad (21)$$

$$\text{CUCCD} = \text{CURL} \times F_3/F_4, \quad (22)$$

$$\text{CNACCD} = (\text{CSCCD} - \text{CKCCD})/2, \quad (23)$$

where F_3 is flow in the loop of Henle, F_4 is the flow out of the cortical collecting duct, CKA is the systemic plasma potassium concentration, TNACCD is the sodium transport rate in the cortical collecting duct, expressed as pmol/min/mm tubular length, LT is the length of the distal tubule-cortical collecting duct segment (10 mm)[16], CURL is urea concentration of the fluid exiting the loop of Henle calculated from Eq. (18) and CSCCD is the osmolality of the fluid exiting the cortical collecting duct calculated using Eq. (20).

Medullary collecting duct

Fluid reabsorption from the medullary collecting duct is driven by the differences in hydrostatic and osmotic forces acting across nodes 8–11 in Fig. 2. The osmotic force PRCD(I) for fluid reabsorption expressed in mmHg at each medullary level was calculated using Eq. (24) below:

$$\text{PRCD}(I) = RT \times \{\text{SSCD} \times [\text{CSI}(I) - \text{CSCD}(I)] + \text{SUCD} \times [\text{CUI}(I)]\} + \text{PONG}, \quad (24)$$

where R is the gas constant, T is absolute temperature, SSCD is the salt reflection coef-

ficient of the medullary collecting duct. CSI(I) is a parameter representing the salt concentration in the medullary interstitium, CSCD(I) is the salt concentration in the medullary collecting duct. SUCD is the urea reflection coefficient of the medullary collecting duct. CUI(I) is a parameter representing the urea concentration of the medullary interstitium, CUCD(I) is the urea concentration of the fluid in the medullary collecting duct and PONG is the colloid osmotic pressure of the plasma in the vasa recta capillaries. PONG was calculated from the arterial protein concentration and the single nephron filtration fraction as has been described previously by others[4, 5]. As discussed earlier, the concentration of urea and salt (primarily sodium chloride) in the interstitium at each medullary level were included in the model as parameters. The concentrations of salt [CSCD(I)] and urea [CUCD(I)] in the lumen of the medullary collecting duct were calculated using Eqs. (25) and (26):

$$\text{CSCD}(I) = [\text{FCDIN}(I) \times \text{CSCDIN}(I) - \text{MSCD}(I)]/\text{FCDIN}(I + 1), \quad (25)$$

$$\text{CUCD}(I) = [\text{FCDIN}(I) \times \text{CSCDIN}(I) - \text{MUCD}(I)]/\text{FCDIN}(I + 1), \quad (26)$$

where FCDIN(I) is the fluid flow rate into the medullary collecting duct segment FCDIN(I + 1) is the volume flow rate out of that tubular segment, CSCDIN(I) is the salt concentration entering the tubular segment, CUCDIN(I) is the urea concentration of the fluid entering the tubular segment, MSCDI is the mass of salt reabsorbed from the collecting duct segment into the medullary interstitium and CUCD(I) is the mass of urea reabsorbed in that tubular segment.

The mass of urea and salt reabsorbed in each medullary collecting duct segment was calculated as follows using Eqs. (27) and (28):

$$\text{MSCDI}(I) = \text{DSCD} \times [\text{CSCD}(I) - \text{CSI}(I)] + \text{FWCDI}(I) \times \text{CSCD}(I) \times (1.0 - \text{SSCD}) + \text{TNAMCD}, \quad (27)$$

$$\text{MUCDI}(I) = \text{DUCD} \times [\text{CUCD}(I) - \text{CUI}(I)] + \text{FWCDI}(I) \times \text{CSCD}(I) \times (1 - \text{SUCD}), \quad (28)$$

where DUCD and DSCD represent the urea and salt diffusion coefficients of the medullary collecting duct, FWCDI(I) is volume reabsorption from the tubular segment derived from the previous solution of the loop flow Eqs. (1)–(8), SSCD and SUCD are the salt and urea reflection coefficients, CSCD(I) and CUCD(I) are the concentrations of salt and urea in the medullary collecting duct and CSI(I) and CUI(I) are the salt and urea concentrations in the medullary interstitium.

As depicted in Fig. 2, fluid and solute reabsorbed from the medullary collecting duct empties into a juxtaposed vasa recta-medullary interstitium node. This reabsorbed fluid exits the medulla to the renal vein through node 14. To make this simplification of the countercurrent system, we assumed that the solute concentration of the vasa recta blood and medullary interstitium rapidly equilibrates and can be represented at any medullary level by a well mixed compartment. This assumption is a direct application of the central core hypothesis proposed by Stephenson *et al.*[1]. Secondly, we assumed that the vasa recta in the steady state must remove from each medullary compartment a quantity of water that exactly equals the fluid reabsorbed from the medullary collecting duct in that segment. Using these assumptions, at steady state solute loss from a medullary interstitial compartment equals the volume flow out of the compartment times the interstitial urea and sodium chloride concentration at the boundary of the comparment.

3. MODEL SOLUTION

The model was solved using an iterative approach outlined in Fig. 3. The cortical and medullary models are loosely coupled and were solved independently. For a given set of parameters and initial estimates for flow in loops 1–4 of the cortical model (Fig. 2), a set of flow dependent equivalent hydrostatic forces for fluid movement were calculated. The network loop Eqs. (1)–(4) were then solved using matrix methods and the new flows F_1–F_4 were used to recalculate forcing functions throughout the cortical model. The cortical solution was allowed to iterate until it converged on a value for flow out of the cortical collecting duct that deviated from the previous estimate by less than 1%. Using this estimate of flow entering the medullary collecting duct, initial values for the various equivalent hydrostatic forces acting across the medullary collecting tubule were calculated and the network Eqs. (5)–(8) were solved. These new estimates of fluid flows into and out of each node were used to recalculate the medullary hydrostatic forcing functions and the medullary solution was allowed to iterate until the calculated urine flow varied by less than 1% from the estimates obtained from the previous solution.

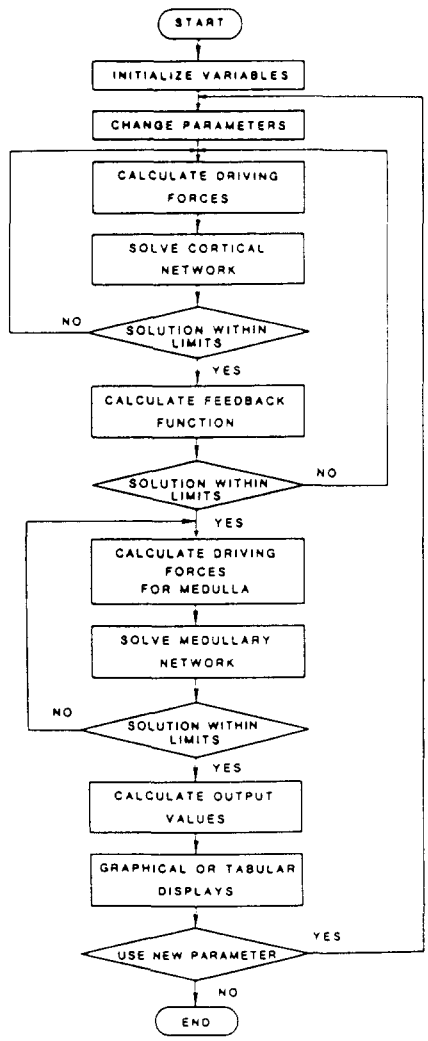

Fig. 3. Flow diagram for the solution of the computer model of a human nephron.

4. RESULTS AND DISCUSSION

Calculated variables

A summary of all predicted variables using the parameters listed in Table 1 are presented in Table 3. The model predictions for urine flow, urine osmolarity, sodium and potassium excretion, glomerular filtration rate and renal blood flow are all within normal limits usually reported for a normally hydrated man eating a typical American diet[23]. The values for tubular fluid flow rates, solute concentrations and tubular hydrostatic pressures throughout the nephron closely agree with micropuncture data previously reported for the dog[20, 24, 25]. We would expect that these predicted single-nephron values apply to man as well, since the tubular diameters and tubular lengths[16], as well as the value of glomerular filtration rate divided by the number of nephrons are similar in both species[23]. Thus, using published values for solute transport rates in various tubular segments of the dog nephron, hydraulic conductivities reported for the rabbit nephron[14, 15], values for the lengths and diameters of various segments of the human nephron[11, 16], as well as measured concentrations for salt and urea at different levels of the medulla of the dog[19], the model quantitatively predicted reasonable values for flows, pressures and solute concentrations throughout the nephron. One important finding was that the model predicted that 65% of the filtered load of water was reabsorbed along the proximal tubule. This is consistent with micropuncture data in rats[9, 21, 22] and dogs[20, 24, 25]. The primary forces we included in the model for fluid reabsorption in the proximal tubule were active bicarbonate reabsorption [Eq. (12)] and the solute asymmetry force [Eq. (14)]. Thus the prediction of normal fractional fluid reabsorption in the proximal tubule is in general agreement with previous conclusions of Warner and Lechene[21] and Andreoli and Schafer[26] suggesting that active transport of bicarbonate in the proximal tubule generates sufficient force to account for most of the fluid reabsorption that occurs in this nephron segment.

Tubuloglomerular feedback control of GFR

Considerable controversy exists over the mechanisms responsible for autoregulation of glomerular filtration rate and renal blood flow. There is evidence that supports the hypothesis that a myogenic vasoconstriction of the afferent arteriole is primarily involved[27–29]. Conversely, other data favors a tubuloglomerular feedback control mechanism for GFR autoregulation. It has been proposed that the loop of Henle flow or some solute concentration in loop fluid is sensed by the cells of the macula densa and that these cells send a message through the juxtaglomerular apparatus that results in adjustments in arteriolar resistance[25, 30–32]. Most of the experimental evidence has suggested that these resistance adjustments occur primarily in the afferent arteriole[30]. Hall *et al.*[33] have emphasized that changes in efferent arteriolar resistance may also be involved. One of the important uses of the renal model was to investigate various hypotheses concerning the mechanism of autoregulation.

Using the model, we evaluated the hypothesis that a feedback control system that sensed loop of Henle flow and adjusted afferent arteriolar resistance was sufficient to explain autoregulation of renal blood flow and glomerular filtration rate in man. This was accomplished by adding an iterative loop to the model which would incrementally increase afferent arteriolar resistance until loop of Henle flow (FHS) was returned to its control value plus or minus an error signal defined by an adjustable feedback gain according to Eq. (29):

$$\mathrm{FHS} = \mathrm{FHIc} + (\mathrm{FHI} - \mathrm{FHIunc})/(1 + \mathrm{GAIN}). \tag{29}$$

Table 3

VARS:			
CPROTG-	7.25696	g/dl	Mean glomerular protein concentration
CSURIN-	189.93440	mEq/l	Salt concentration in urine
CUURIN-	315.35930	mmol/l	Urea concentration in urine
CSI1 -	400.00000	mEq/l	Interstitial block 1 med. salt conc.
CSI2 -	448.00000	mEq/l	Interstitial block 2 med. salt conc.
CSI3 -	496.00000	mEq/l	Interstitial block 3 med. salt conc.
CSI4 -	544.00000	mEq/l	Interstitial block 4 med. salt conc.
CUI1 -	50.00000	mmol/l	Interstitial block 1 med. urea conc.
CUI2 -	170.00000	mmol/l	Interstitial block 2 med. urea conc.
CUI3 -	290.00000	mmol/l	Interstitial block 3 med. urea conc.
CUI4 -	410.00000	mmol/l	Interstitial block 4 med. urea conc.
CSCD1 -	97.87453	mEq/l	Collecting duct block 1 med. salt conc.
CSCD2 -	101.84180	mEq/l	Collecting duct block 2 med. salt conc.
CSCD3 -	115.89160	mEq/l	Collecting duct block 3 med. salt conc.
CSCD4 -	158.11780	mEq/l	Collecting duct block 4 med. salt conc.
CUCD1 -	166.83600	mmol/l	Collecting duct block 1 med. urea conc.
CUCD2 -	181.94480	mmol/l	Collecting duct block 2 med. urea conc.
CUCD3 -	210.58340	mmol/l	Collecting duct block 3 med. urea conc.
CUCD4 -	272.38730	mmol/l	Collecting duct block 4 med. urea conc.
CINCCD-	48.55908	mosm/l	Osmol. conc. input to cortical col. duct
CSCCD -	259.08120	mosm/l	Osmotic conc. leaving cortical col. duct
CHCO3A-	24.02296	mEq/l	Arterial bicarbonate concentration
CKCCD -	33.89401	mEq/l	Potassium conc. leaving cort. coll. duct.
CKURIN-	48.70658	mEq/l	Potassium concentration in urine
CNURIN-	46.26062	mEq/l	Sodium concentration in urine
CURL -	30.27597	mmol/l	Urea concentration leaving loop of Henle
DDNACL-	5153.25400	pmol/min	Distal delivery of NaCl
EXK -	43.11718	pEq/min	Single nephron potassium excretion
EXNA -	40.95191	pEq/min	Single nephron sodium excretion
EXUR -	279.16970	pmol/min	Single nephron urea excretion
FSNRBF-	466.30900	nl/min	Single nephron renal blood flow
FEFF -	412.80490	nl/min	Single nephron efferent blood flow
FGFR -	53.50410	nl/min	Single nephron glomerular filt. rate
FHENLE-	18.40448	nl/min	Single nephron loop-of-Henle flow
FFRACT-	.20862		Filtration fraction
FWPI -	35.09962	nl/min	Flow of water from prox. tub. to interstit.
FWCDI1-	.41229	nl/min	Water flow from CD block 1 to interstitium
FWCDI2-	.59079	nl/min	Water flow from CD block 2 to interstitium
FWCDI3-	.74194	nl/min	Water flow from CD block 3 to interstitium
FWCDI4-	.81925	nl/min	Water flow from CD block 4 to interstitium
FURINE-	.88524	nl/min	Single nephron urine flow
FCCD -	3.44952	nl/min	Flow out of the cortical collecting duct
GFR -	128.40990	ml/min	Total renal glomerular filtration rate
RBF -	1119.14200	ml/min	Total renal blood flow
UF -	2.12458	ml/min	Total urine flow
LBPT -	3.21332	mm	Length of prox. tubule for bicarb. reab.
LANACL-	4963.99900	pmol/min	Loop of Henle absorption of NaCl
OURINE-	505.29370	mosm/l	Urine osmotic concentration
PASSYP-	190.43170	mmHg	Prox. pressure due to solute assymetry
PONCG -	23.16293	mmHg	Mean oncotic pressure in glomerulus
PCDIN -	1.37981	mmHg	Effective force driving medullary system
PCTDD -	34.39826	%	Percent distal delivery
PCTDR -	27.95106	%	Percent distal reabsorption
PCTPR -	65.60175	%	Percent proximal reabsorption
PCTFE -	1.65453	%	Percent fractional excretion
PGLOM -	53.36910	mmHg	Mean glomerular hydraulic pressure
PPROX -	16.11395	mmHg	Proximal tubule hydraulic pressure
PDIST -	6.91171	mmHg	Distal tubule hydraulic pressure
PPERI -	24.53155	mmHg	Peritubular cap. hydraulic pressure
PNAP -	97.49972	mmHg	Prox. pressure due to sodium
PSCCD -	2821.27100	mmHg	Pressure due solute in cor. coll. duct
PCI -	3.44205	mmHg	Pressure in cortical interstitium
PHCO3P-	98.28944	mmHg	Prox. pressure due to bicarbonate
TEXK -	103.48120	uEq/min	Total renal excretion of potassium
TEXNA -	98.28458	uEq/min	Total renal excretion of sodium
TEXUR -	670.00740	umol/min	Total renal excretion of urea
TAB -	1285.32700	pEq/min	Total prox. absorption of bicarbonate
TTNAP -	1275.00000	pEq/min	Total amount of Na transported in prox. tub.

where FHIc is the set point for loop of Henle flow rate, FHI is the new value of loop of Henle flow after a parameter change and GAIN represents the strength of the tubular-glomerular feedback loop. The results of the model predictions for renal blood flow, glomerular filtration rate, urine flow and sodium excretion over a range of arterial pressures, with and without feedback control of glomerular filtration rate, are presented in Fig. 4. The model predicts that in the absence of the tubuloglomerular feedback control system, renal blood flow, glomerular filtration rate, urine flow and sodium excretion would increase as arterial pressure was elevated. Addition of the tubuloglomerular feedback

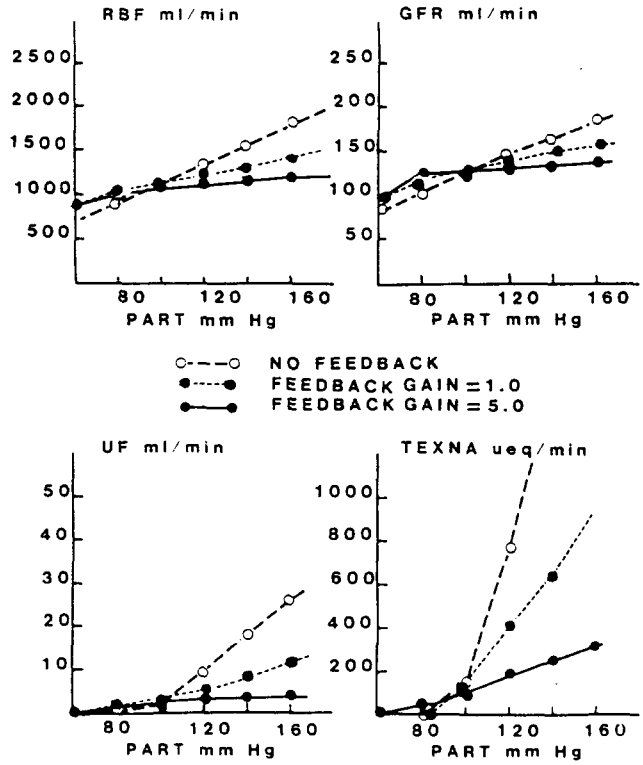

Fig. 4. Predicted relationships between renal blood flow (RBF), glomerular filtration rate (GFR), urine flow (UF), sodium excretion (TexNa) and renal perfusion pressure (PART) in the presence and absence of a tubular glomerular feedback control of GFR.

system with a gain of 5 or higher was sufficient to explain the near constancy of glomerular filtration rate and renal blood flow over a range of perfusion pressures from 80 to 160 mmHg. Using a lower feedback gain of 1, which is consistent with the strengths of many physiological control systems, blood flow and glomerular filtration rate were not well controlled and increased to a greater extent than that usually seen in experimental studies[28, 30, 33]. Although a relatively high gain (5 or greater) was needed to explain autoregulation of renal blood flow and glomerular filtration rate via a glomerulotubular feedback system, it should be noted that a recent study of Moore[34] suggests that the effective gain of this system may be as high as 40 in rats.

Hormonal control

The major hormones regulating renal function are vasopressin, aldosterone and the renin-angiotensin system. In addition, numerous studies indicate that the renal sympathetic nerves modulate proximal tubular reabsorption of solute and water in addition to their effect on renal hemodynamics. Based on the reported physiological action of these neural and hormonal controllers of kidney function, we have developed equations to put some of the model parameters under hormonal control. A description of these equations and examples of the predicted effect of changes in the activity of these neural and hormonal controllers on renal function are given below.

Vasopressin

We have assumed that vasopressin regulates water excretion by influencing the water permeability of the cortical (KDIST) and the medullary collecting duct (KCD) as well as the magnitude of the cortico-medullary urea and salt gradients, DELUI and DELSI, respectively. The ability of vasopressin to increase the water permeability of the cortical and medullary collecting duct is well known and has been repeatedly demonstrated with both *in vivo* and *in vitro* experiments[14, 16, 18]. Increases in plasma vasopressin levels over the physiologic range have also been reported to produce approximately a 50% increase in salt concentration and a fourfold increase in urea concentration in the medullary interstitium of the dog[19].

The exact nature of the relationship between plasma vasopressin levels and hydraulic conductivity of the collecting duct, however, is unknown. In man, urine osmolarity is minimal (approximately 50 mOsmol/l) at plasma vasopressin levels of 0.5 pg/ml and rises to a maximum of approximately 1000 mOsmol/kg·H_2O, at plasma vasopressin concentrations of 5.0 pg/ml[35]. In isolated, perfused rat cortical collecting ducts, Reif *et al.*[36] have recently reported that osmotic water permeability increases in a log dose response manner over a range of vasopressin concentrations of 3–40 pg/ml. However, these *in vitro* actions of vasopressin on the collecting duct appear to occur at doses greater than the physiologic range for man or rats. In the absence of any data for man, we assumed that linear relationships exist between plasma vasoppressin concentration, hydraulic conductivities of the cortical and medullary collecting duct and the medullary salt and urea gradients. Equations (30)–(33) below describe the incorporation of vasopressin control of water excretion into the present model:

$$\text{KDIST} = 0.001 + 0.1*\text{HADH}/5.0, \tag{30}$$

$$\text{KCD} = 0.0001 + 0.005*\text{HADH}/5.0, \tag{31}$$

$$\text{DELSI} = 30 + 30 \times \text{HADH}/5.0, \tag{32}$$

$$\text{DELUI} = 20 + 100 \times \text{HADH}/5.0. \tag{33}$$

KDIST represents the filtration coefficient of the cortical collecting duct, KCD is the filtration coefficient of the medullary collecting duct, DELSI is the salt gradient expressed in mEq/l in the inner medulla and DELUI is the urea gradient in the inner medulla expressed in mmol/l. The minimum and maximum values for these parameters are as follows:

$$0.001 \leq \text{KDIST} \leq 0.008,$$

$$0.001 \leq \text{KCD} \leq 0.0006,$$

$$30 \leq \text{DELSI} \leq 60,$$

$$20 \leq \text{DELUI} \leq 100.$$

The predicted relationships between urine flow, urine osmolarity and plasma vasopressin levels are presented in Fig. 5. The model accurately predicts that urine flow decreases and urine osmolarity increases as vasopressin levels are varied within the physiological range from 0.5 to 10 pg/ml. Minimal urine osmolarity was predicted to be 50 mOsmol/kg·H_2O. Even though the four parameters under vasopressin control were linearly equated with plasma vasopressin concentration, the model indicated that the expected relationship between urine osmolarity and plasma vasopressin level was curvilin-

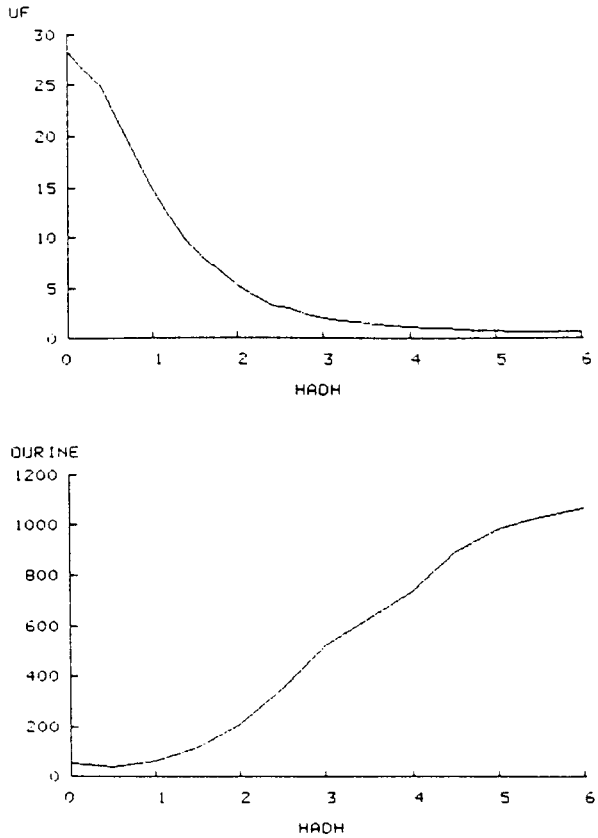

Fig. 5. Predicted effect of vasopressin (HADH) expressed in pg/ml on urine flow (UF) expressed in ml/min and urine osmolality (OURINE) expressed in mOsmol/Kg·H_2O.

ear. This result is a consequence of the complex nonlinear flow rate dependence of the forces that drive fluid flows throughout the model. Confirmation of this prediction of the model, however, must await further studies since the relationship between urine osmolarity and plasma vasopressin levels has not yet been experimentally determined in man[35].

Aldosterone

Aldosterone has been shown to regulate the rate of sodium reabsorption and potassium secretion in the cortical collecting duct[14, 15, 37]. The influence of aldosterone on sodium and potassium transport along the medullary collecting duct is unclear. Sodium and potassium reabsorption has been demonstrated in this nephron segment[38, 39]. It is also relatively well known that alterations in medullary collecting duct transport of these ions is important in determining the sodium and potassium excretory response to changes in the volume status of an animal[40]. However, it has not been possible to demonstrate that these changes in medullary collecting duct function are related to alterations in plasma aldosterone concentration[40]. In one study, Sonnenberg reported that the inhibition of medullary collecting duct sodium reabsorption during volume expansion was not influenced by mineralocorticoid levels[40]. Part of the problem may be related to limitations in studying the papillary collecting duct *in vivo*. That is, exposure of the papilla for micropuncture, which impairs the urinary concentrating mechanism, may trigger the release

of prostanoids or kinins which mask the influence of aldosterone on the medullary collecting duct. Nevertheless, despite the lack of positive experimental data to support our hypothesis, we have assumed that sodium reabsorption in the medullary collecting duct is directly related and potassium reabsorption is inversely related to plasma aldosterone concentration.

Very little experimental data exists on the relationship between sodium and potassium transport in the collecting duct and plasma aldosterone concentration in man or animals. In the absence of this crucial information, we assumed that the rates of sodium-potassium exchange in the cortical collecting duct are linearly related to aldosterone levels and can be expressed by Eq. (34):

$$\text{TNACCD} = 0.1 + 0.5 \times \text{HALDO}/10.0, \tag{34}$$

where TNACCD is the rate of sodium reabsorption and potassium secretion in the cortical collecting duct and are expressed in pmol/min/mm tubular length. HALDO is the plasma level of aldosterone expressed in ng/dl and 10 represents the normal circulating plasma aldosterone concentration in man[39]. The rate of sodium reabsorption in all medullary collecting ducts, TNAMCD expressed in pmol/min/mm length of the papilla was assumed to also be related to plasma aldosterone levels using Eq. (35). The slopes of these relationships were empirically determined to mimic experimental data in the dog indicating that a tenfold rise in sodium excretion was associated with approximately a 50% fall in plasma levels of aldosterone[42]:

$$\text{TNAMCD} = 5 + 35.0 \times \text{HALDO}/10.0. \tag{35}$$

In addition to influencing sodium transport in the distal nephron as discussed earlier, aldosterone also regulates the rate of potassium secretion in the cortical collecting duct. This influence of aldosterone on potassium transport was modeled as follows. We assumed that potassium delivery to the cortical collecting duct could be calculated as follows:

$$K \text{ delivery} = \text{CKA} \times \text{FHI}, \tag{36}$$

where CKA is the arterial potassium concentration (mEq/l) and FHI is the loop of Henle flow expressed in ml/min. We assumed that the rate of potassium secretion in the cortical collecting duct was equal and opposite to the rate of sodium reabsorption (TNACCD)[14, 15]. The reabsorption of sodium in the cortical collecting duct (TNACCD) is under the control of aldosterone as defined by Eq. (34). The concentration of potassium leaving the cortical collecting duct (CKCCD) was calculated using Eq. (37):

$$\text{CKCCD} = (\text{CKA} + \text{TNAMCD} \times \text{LT}) \times \text{FHI}/\text{FCCD}, \tag{37}$$

where CKA is arterial potassium concentration, TNAMCD represents the potassium secretion rate in pmol/min·mm tubule, LT is the length of the distal tubule-cortical collecting duct nephron segment[16], FHI is the flow rate entering the cortical collecting duct and FCCD is the flow rate leaving the duct in nl/min.

In the medullary collecting duct, micropuncture studies by Dietz *et al.*[43] indicate that approximately 50% of the delivered load of potassium is reabsorbed. As discussed above, we have assumed that potassium reabsorption in the medullary collecting duct would be inversely related to plasma levels of aldosterone and can be defined by Eq. (38) below:

$$\text{TKMCD} = 5000/\text{TNAMCD} + 20, \tag{38}$$

where TKMCD is the rate of potassium reabsorption in the medulla in pmoles/min/medullary segment. 5000 pmoles of potassium reabsorption per medullary segment represents an empirically determined constant. TNAMCD is the rate of sodium reabsorption which is directly related to plasma levels of aldosterone through Eq. (35).

The predicted relationship between the total renal excretion of both sodium and potassium as a function of plasma aldosterone concentration is depicted in Fig. 6. In accord with experimental data in the dog[41, 42, 44], the model predicts that sodium excretion declines and potassium excretion increases as plasma levels of aldosterone are elevated. We recognize that the model predicts that sodium and potassium excretion are very sensitive to plasma levels of aldosterone. This is consistent with the data of Young *et al.*[42] in the dog. However, we expect that as data becomes available concerning the exact relationship between plasma aldosterone levels and sodium and potassium excretion in man, possible adjustments in the slopes of Eqs. (34) and (35) will be required so that model prediction better fit human experimental data.

Renin-angiotensin system

The renin-angiotensin system has been shown by Hall *et al.*[33] to exert an important influence on the vascular tone of the efferent arteriole. It also has been recently reported

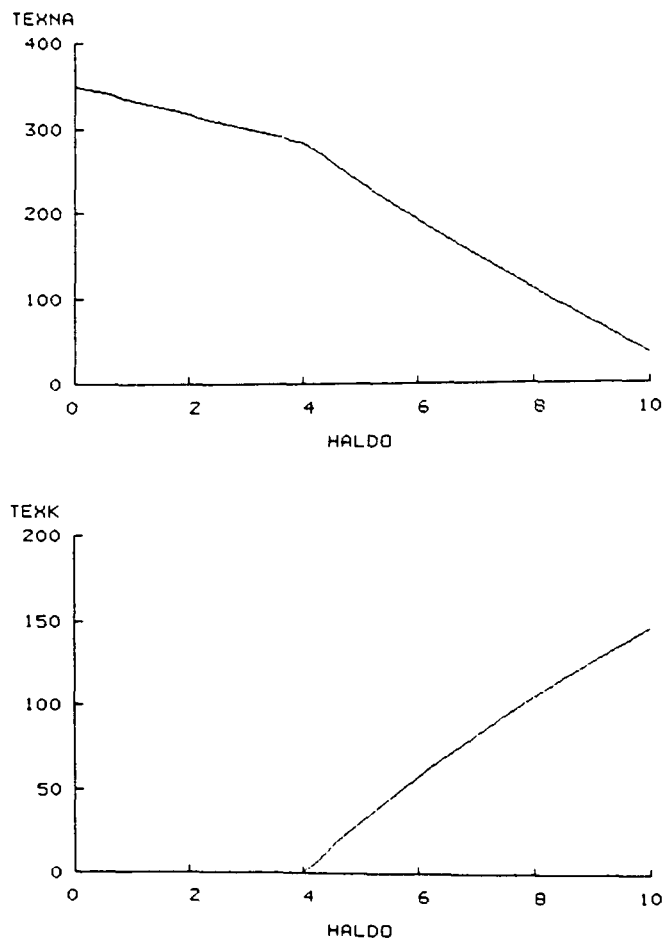

Fig. 6. Predicted effect of aldosterone (HALDO) expressed in ng/dl on sodium (TEXNA) excretion expressed in uEq/min and potassium (TEXK) excretion expressed in uEq/min.

that the afferent arteriolar tone also increased when plasma renin levels are elevated[44, 45]. We have modeled these actions of the renin-angiotensin system using the following equations:

$$\text{REFF} = 0.03 + 0.04 \times \text{HPRA}/2.0, \tag{39}$$

$$\text{RAFF} = 0.05 + 0.2 \times (\text{HPRA} - 4.0), \tag{40}$$

where REFF is efferent arteriolar resistance, RAFF is the afferent arteriolar resistance, HPRA is the plasma renin activity expressed as ngAI/ml/3h. 2.0 ngAI/ml/3h was taken as normal plasma renin activity. The minimum and maximum allowable values for REFF and RAFF were

$$0.30 \leq \text{REFF} \leq 0.07,$$

$$0.05 \leq \text{RAFF} \leq 1.0.$$

Our initial analysis demonstrated that a high gain tubuloglomerular feedback system for control of glomerular filtration rate that adjusts afferent arteriolar resistance would override the vasoconstrictor action of the renin-angiotensin system. It became clear that the renin-angiotensin system must do more than simply affect the tone of the afferent and efferent arterioles in order to explain its effect on renal blood flow and glomerular filtration rate in the presence of a feedback system. In attempting to model the vasoconstrictor actions of the renin-angiotensin system, we have hypothesized that the renin-angiotensin system alters the set point of tubuloglomerular feedback system according to Eq. (41) below:

$$\text{FHI} = \text{FHI} - (\text{HPRA} - 4.0), \tag{41}$$

where FHI is the controlled value for loop of Henle flow in nl/min and HPRA is the plasma renin activity in ngAI/ml/3h. The predicted relationships between plasma renin activity and renal blood flow, glomerular filtration rate, urine flow and sodium excretion are presented in Fig. 7. At plasma renin activity levels between 0 and 2 ngAI/3h, plasma renin activity primarily affected the filtration fraction. Glomerular filtration rate increased, and renal blood flow decreased as plasma renin activity was elevated. As plasma renin levels were increased further, both renal blood flow and glomerular filtration rate were reduced. The fall in glomerular filtration rate produced a marked decrease in urine flow and sodium excretion. Overall, these results resemble dose-related renal effects of angiotensin II in the dog[33, 46] and indicate that most of the actions of the renin-angiotensin system can probably be explained by its ability to regulate renal vascular tone. While there is some recent evidence to indicate that the activity of the renin-angiotensin system influences the strength of the tubuloglomerular feedback response[45, 47], it remains to be demonstrated experimentally whether it also affects the setpoint of the feedback system as the model suggests it might.

Renal nerve activity

Low-frequency renal nerve stimulation at 1–4 Hz has been shown to enhance proximal tubular reabsorption of sodium and water[48]. The mechanism for this neurogenic enhancement of sodium reabsorption is unknown, but recent preliminary data by Osborn and Roman[49] indicates that the renal nerves may affect fluid reabsorption in the proximal tubule by increasing bicarbonate reabsorption through stimulation of Na–H exchange.

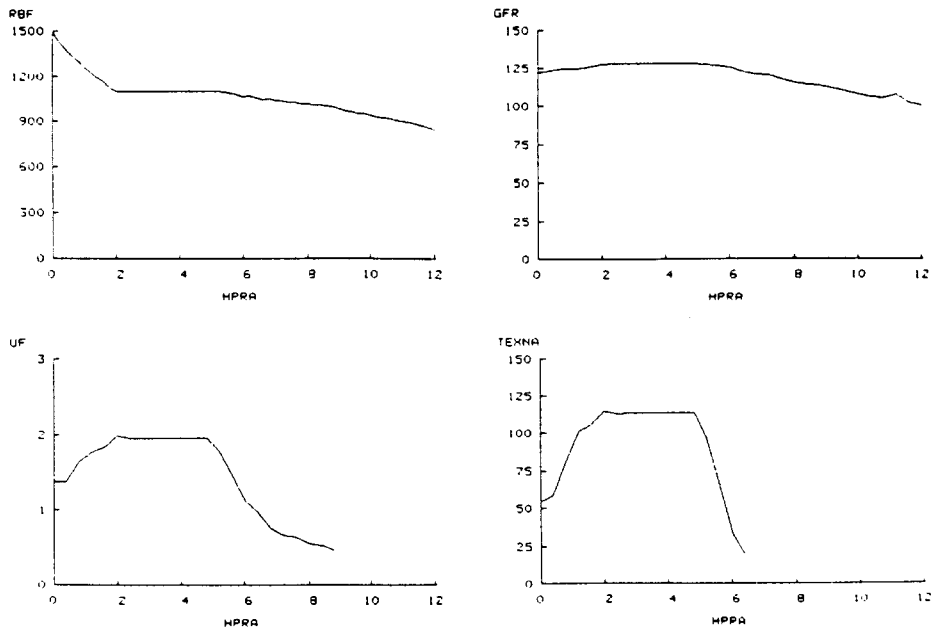

Fig. 7. Predicted effect of plasma renin activity (HPRA) expressed in ngAIformed/3h on renal blood flow (RBF) expressed in ml/min, glomerular filtration rate expressed in ml/min, sodium excretion (TEXNA) expressed in uEq/min and water excretion (UF) expressed in ml/min.

We have tested this hypothesis using the model by assuming that renal nerve activity influences the transport rate of bicarbonate in the proximal tubule according to Eq. (42):

$$\text{THCO3P} = 100 + (300 \times \text{NRNA}) \tag{42}$$

where THCO3P is the rate of sodium bicarbonate reabsorption in the proximal tubule expressed as pmoles/min/mm lenght of tubule, and NRNA is the renal nerve activity expressed as a factor times the normal value of 1. Proximal tubular reabsorption of sodium bicarbonate was allowed to vary over a range of 0 to 600 pmole/min/mm length of tubule.

High levels of renal nerve stimulation in the 4–10-Hz range also has been shown to lower renal blood flow and glomerular filtration rate by constricting the afferent arteriole[48]. These actions of the renal nerves were modeled using Eq. (43):

$$\text{RAFF} = 0.05 + 0.2 \times (\text{NRNA}/4.0), \tag{43}$$

where RAFF is afferent arteriolar resistance, and NRNA is the level of renal nerve activity. In the presence of tubuloglomerular feedback system for the control of GFR; however, Eqs. (42) and (43) proved insufficient to mimic the ability of renal nerve stimulation to lower renal blood flow. As proximal tubular reabsorption increased or glomerular filtration rate was reduced by stimulation of the renal nerves, the feedback system attempted to compensate by decreasing afferent arteriolar tone. In order to adequately simulate the action of the renal nerves or renal blood flow, we proposed that renal nerves affect the set point of tubular glomerular feedback according to Eq. (44):

$$\text{FHI} = \text{FHI} - (\text{NRNA} - 1), \tag{44}$$

where FHI is the controlled value for loop of Henle flow expressed in nl/min. This flow

rate was allowed to vary over a range of values from 1 to 18.5 nl/min. The predicted relationships between renal sympathetic nerve activity (NRNA) and renal blood flow, glomerular filtration rate, urine flow and sodium excretion are presented in Fig. 8. As the renal nerve activity was increased above normal, both urine flow and the total renal excretion of sodium fell markedly with little change in renal hemodynamics. At higher levels of renal nerve activity, both renal blood flow and glomerular filtration rate began to fall. These results are qualitatively in line with the results of many experiments in the dog reviewed by DiBona[48]. Our hypothesis that renal nerves must affect the set point of the tubuloglomerular feedback system is consistent with recent findings of Osborn *et al.*[50] who found that during nerve stimulation, the kidney of the dog autoregulated renal blood flow and glomerular filtration rate at a lower level of flow. More direct experimental data will be needed to evaluate our hypothesis that the renal nerves modulate the setpoint of the tubuloglomerular feedback system.

Effect of furosemide on renal concentrating ability

To further evaluate the ability of the kidney model to predict changes in renal function when more than one parameter was altered simultaneously, we studied the effect of furosemide on urinary concentrating ability. The results of these experiments are presented in Fig. 9. As discussed earlier, urine flow decreased and urine osmolarity increased when plasma vasopressin levels were varied from 1 to 10 pg/ml. The effect of furosemide was superimposed on this relationship by lowering the transport rate of sodium chloride in the loop of Henle (TNAH) from 1000 to 200 pmoles/min/mm tubular length. Furosemide administration produced a large increase in urine flow and blocked the ability of vasopressin to concentrate the urine. After furosemide, urine osmolarity ranged between 300 and 500 mOsmol/kg·H_2O regardless of the plasma level of vasopressin. Thus the renal model accurately predicted the diuretic-natriuretic effect of lowering the loop of Henle

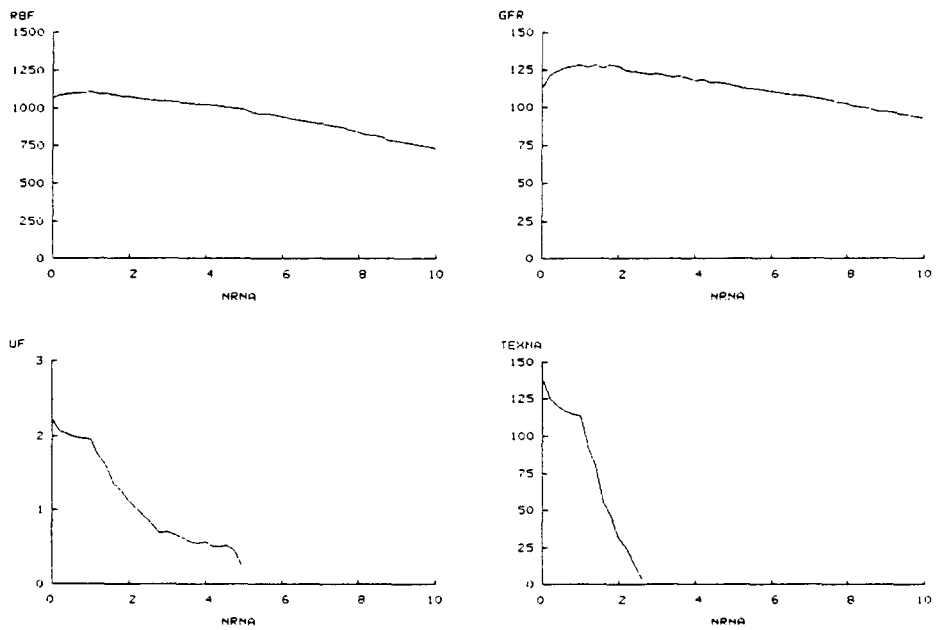

Fig. 8. Predicted effect of renal nerve activity (NRNA) expressed as activity times normal on renal blood flow (RBF) (units ml/min), glomerular filtration rate (GFR) (units ml/min), urine flow (UF) (units ml/min) and sodium excretion (TEXNA) (units uEq/min).

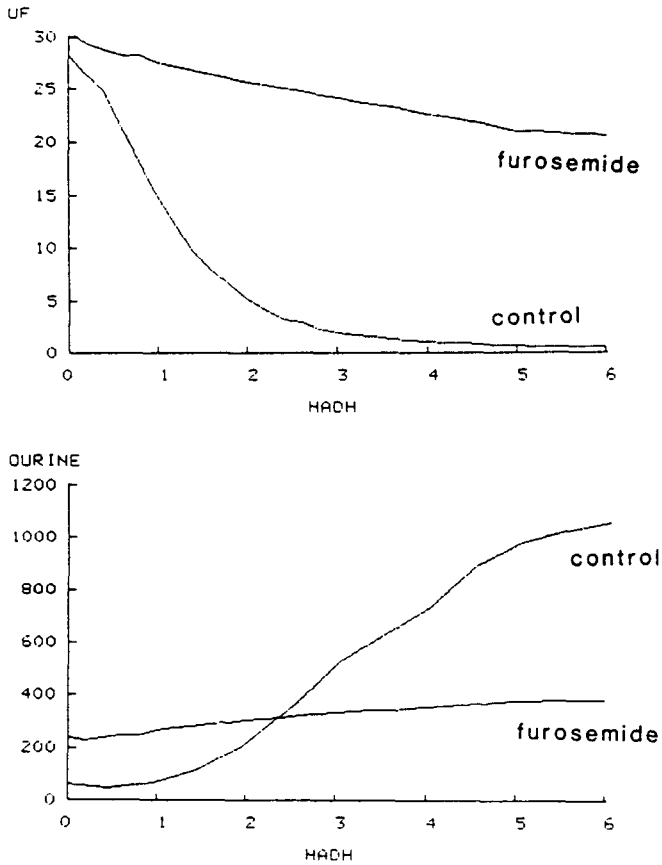

Fig. 9. Effect of furosemide on urine flow (UF) (units ml/min) and urine osmolality (OURINE) (units mOsmol/kg·H_2O) as a function of plasma vasopressin concentration (HAHD) expressed in pg/ml.

transport constant with furosemide as well as indicating that this drug prevents formation of either a concentrated or a dilute urine[51].

Glomerular injury

Our final simulation was performed to illustrate the usefulness of the kidney model to study the overall effect of multiple changes in renal parameters which often occur in the course of a disease process. For this example, we have chosen to evaluate the effect of lowering the ultrafiltration coefficient of the glomerulus (KFGLOM) by 50% on renal blood flow, glomerular filtration rate, urine flow and sodium excretion. A fall in the ultrafiltration coefficient of the glomerulus is thought to be the underlying cause of several forms of acute and chronic renal failure[52, 53]. The results of these experiments are presented in Fig. 10. Lowering the glomerular ultrafiltration coefficient resulted in a lowering of glomerular filtration rate, urine flow and sodium excretion at any level of arterial pressure. Renal blood flow increased because the tubuloglomerular feedback system compensated for the reduced KFGLOM by reducing afferent arteriolar resistance to its minimum value in an attempt to normalize glomerular filtration rate. The resultant rise in glomerular capillary pressure would be detrimental to the kidney, tending to destroy glomeruli and augmenting nephron loss.

Eventually, the reduced output of sodium and water in these patients with compromised renal function would result in a slight volume expansion that would suppress plasma levels

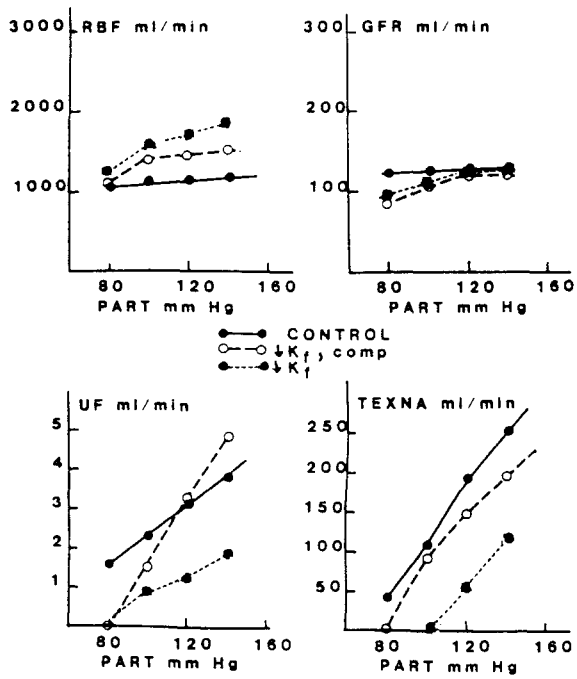

Fig. 10. Effect of lowering the glomerular filtration coefficient (KFGLOM) on renal function before and after hormonal compensation for the renal injury.

of vasopressin, aldosterone and renin[54]. Also shown in Fig. 10 are the results of another simulation representing the steady-state condition after the renal hormones were allowed to compensate for glomerular injury. As can be seen in Fig. 10, after vasopressin, aldosterone, and renin levels were suppressed, urine flow and sodium excretion returned toward control despite the fact that the glomerular filtration rate remained suppressed. These results approximate the initial and long-term effects of glomerular injury that have been previously described[52–54].

5. CONCLUSIONS

In summary, we have described a compartmentalized computer model of the human kidney that incorporates feedback control of glomerular filtration rate as well as neural and hormonal control of renal function. Using published values of solute transport rates in individual nephrons, published hydraulic single-nephron permeabilities, tubular lengths and diameters, the model quantitatively predicted urine flow, sodium and potassium excretion, renal blood flow, glomerular filtration rate, etc., for any given level of arterial pressure and neural and hormonal input to the kidney. The model appeared to accurately predict the changes in renal function produced by changes in renal hormone levels. It also was useful to describe those changes in renal function known to occur after administration of diuretic drugs or that are associated with many disease states. By changing a few parameters, such as ultrafiltration coefficients and number of nephrons, this same renal model can be used to simulate the kidney of rats and dogs as well as humans. The renal model is available from the authors on diskettes and can be run on a variety of personal computers using the MS-DOS or PC-DOS operating systems. This model should be useful as a research tool to help evaluate hypotheses concerning the control of renal function as well as to predict changes in kidney function expected during disease states

when renal hormone levels and other determinants of renal function are simultaneously altered. This model should also be useful in teaching renal physiology and the underlying causes of renal disease after being coupled to a computer-based instruction subroutine we are developing.

Acknowledgements—The authors wish to thank Ms. Kathy Feil for her excellent secretarial assistance. We also wish to thank Dr. Ed Quillen and Dr. B. J. Barber for their assistance in developing some of the graphics software used with the model and Dr. A. W. Cowley, Jr., Dr. Jeffrey Osborn and Dr. L. G. Navar for suggestions concerning the model and for critical review of the manuscript. The work was supported in part by grants AG01794 from the National Institute on Aging and HL29587 from the National Heart and Lung Institute. The work was also supported by the NCR Corporation who made a personal computer available for much of the software development.

REFERENCES

1. J. L. Stephenson, Concentrating engines and the kidney: I. Central core model of renal medulla. *Biophys. J.* **13**, 512–545 (1973).
2. T. L. Pallone, T. I. Morgenthaler and W. M. Deen, Analysis of microvascular solute and water exchanges in the renal medulla. *Am. J. Physiol.* **247**, F303–F315 (1984).
3. D. M. Foster and J. A. Jacquez, Comparison using a central core model of the renal medulla of the rabbit and rat. *Am. J. Physiol.* **234**, F402–F414 (1978).
4. L. C. Moore, D. J. Marsh and C. M. Martin, Loop of Henle during the water-to-diuresis transition in Brattleboro rats. *Am. J. Physiol.* **239**, F72–F83 (1980).
5. V. M. Sanjana, P. A. Johnston, C. R. Robertson and R. L. Jamison, An examination of transcapillary water flux in renal inner medulla. *Am. J. Physiol.* **231**, 313–318 (1978).
6. D. J. Marsh and L. E. Segal, Analysis of countercurrent diffusion exchange in blood vessels of the renal medulla. *Am. J. Physiol.* **221**, 817–828 (1971).
7. R. E. Huss and D. J. Marsh, A model of NaCl and water flow through paracellular pathways of renal proximal tubules. *J. Membr. Biol.* **23**, 305–347 (1975).
8. H. Sackin and E. L. Boulpap, Models for coupling of salt and water transport. *J. Gen. Physiol.* **66**, 671–733 (1975).
9. R. R. Warner, T. Strunk and C. Lechene, Analysis of proximal tubule salt and water transport in standing droplets. *J. Theor. Biol.* **77**, 453–471 (1979).
10. J. A. Jacquez and B. Carnahan, A model of the renal cortex and medulla. *Math. Biosci.* **1**, 227–261 (1967).
11. E. Koushanpour, R. R. Tarica and W. F. Stevens, Mathematical simulation of normal nephron function in rat and man. *J. Theor. Biol.* **31**, 177–214 (1971).
12. J. L. Stephenson, R. Mejia and R. P. Tewarson, Model of solute and water movement in the kidney. *Proc. Natl. Acad. Sci. USA* **73**, 252–256 (1976).
13. R. Kainer, A functional model of the rat kidney. *J. Math. Biol.* **7**, 57–94 (1979).
14. H. R. Jacobson, Functional segmentation of the mammalian nephron. *Am. J. Physiol.* **241**, F203–F218 (1981).
15. M. Knepper and M. Burg, Organization of nephron function. *Am. J. Physiol.* **244**, F579–F589 (1983).
16. C. Rouiller and A. F. Muller, *The Kidney*, Vol. 1, pp. 98–99. Academic, New York (1969).
17. M. A. Knepper, R. A. Danielson, G. M. Saidel and R. S. Post, Quantitative analysis of renal medullary anatomy in rats and rabbits. *Kidney Int.* **12**, 313–323 (1977).
18. R. L. Jamison and W. Kriz, *Urinary Concentrating Mechanism*. Oxford University Press, New York (1982).
19. B. Schmidt-Nielsen and R. R. Robinson, Contribution of urea to urinary concentrating ability in the dog. *Am. J. Physiol.* **218**, 1363–1369 (1970).
20. N. L. M. Wong and G. A. Quamme, Tubular handling of bicarbonate in the dog. *Am. J. Physiol.* **241**, F219–F223 (1981).
21. R. R. Warner and C. Lechene, Analysis of standing droplets in rat proximal tubules. *J. Gen. Physiol.* **79**, 709–735 (1982).
22. R. Green and G. Giebisch, Ionic requirements of proximal tubular sodium transport. I. Bicarbonate and chloride. *Am. J. Physiol.* **229**, 1205–1215 (1975).
23. H. Valtin, *Renal Function*. Little, Brown and Company, Boston (1973).
24. G. R. Marchand, Interstitial pressure during volume expansion at reduced renal artery pressure. *Am. J. Physiol.* **235**, F209–F212 (1978).
25. L. G. Navar, P. D. Bell and T. J. Burke, Autoregulatory response of superficial nephrons and their association with sodium excretion during arterial pressure alterations in the dog. *Circ. Res.* **41**, 487–495 (1977).
26. T. E. Andreoli and J. A. Schafer, Effective luminal hypotonicity: the driving force for isotonic proximal tubular fluid absorption. *Am. J. Physiol.* **236**, F89–F96 (1979).
27. J. P. Gilmore, K. G. Cornish, S. D. Rodgers and W. L. Joyner, Direct evidence for myogenic autoregulation in the hamster. *Circ. Res.* **47**, 226–230 (1980).
28. D. K. L. Young and D. J. Marsh, Pulse wave propagation in rat renal tubules: implications for GFR autoregulation. *Am. J. Physiol.* **240**, F446–F458 (1981).
29. L. C. Moore, J. Schnermann and S. Yarimizu, Feedback mediation of SNGFR autoregulation in hydropenic and DOCA- and salt-loaded rats. *Am. J. Physiol.* **237**, F63–F74 (1979).

30. L. G. Navar, D. W. Ploth and P. D. Bell. Distal tubular feedback control of renal hemodynamics and autoregulation. *Annu. Rev. Physiol.* **42**, 557–571 (1980).
31. L. G. Navar, B. Chomdej and P. D. Bell. Absence of estimated glomerular capillary pressure autoregulation during interrupted distal delivery. *Am. J. Physiol.* **229**, 1596–1603 (1975).
32. R. C. Blantz and K. S. Konne. Relation of distal tubular delivery and reabsorption rate to nephron filtration. *Am. J. Physiol.* **233**, F315–F324 (1977).
33. J. E. Hall, A. C. Guyton, T. E. Jackson, T. G. Coleman, T. E. Lohmeier and N. C. Trippodo. Control of glomerular filtration rate by the renin angiotensin system. *Am. J. Physiol.* **233**, F366–F372 (1977).
34. L. C. Moore. Tubuloglomerular feedback and SNGFR autoregulation in the rat. *Am. J. Physiol.* **247**, F267–F276 (1984).
35. A. W. Cowley, Jr.. Vasopressin and cardiovascular regulation. In *International Review of Physiology, Vol. 26* (Edited by A. C. Guyton and J. A. Hall), pp. 189–242. University Park, Baltimore (1982).
36. M. C. Reif, S. L. Troutman and J. A. Schafer. Sustained response to vasopressin in isolated rat cortical collecting tubule. *Kidney Int.* **26**, 725–732 (1984).
37. G. J. Schwartz and M. Burg. Mineralocorticoid effects on cation transport by cortical collecting tubules in vitro. *Am. J. Physiol.* **235**, F576–F585 (1978).
38. R. L. Jamison, J. Buerkert and F. Lacy. A micropuncture study of collecting tubule function in rats with hereditary diabetes insipidus. *J. Clin. Invest.* **50**, 2444–2452 (1971).
39. H. J. Reineck, R. W. Osgood and J. H. Stein. Net potassium addition beyond the superficial distal tubule of the rat. *Am. J. Physiol.* **235**, F104–F110 (1978).
40. H. Sonnenberg. Effect of adrenalectomy on medullary collecting duct function in rats before and after blood volume expansion. *Pflugers Arch.* **368**, 55–62 (1977).
41. A. W. Cowley, Jr., D. C. Merrill, E. W. Quillen, Jr. and M. M. Skelton. Long-term blood pressure and metabolic effects of vasopressin with servo-controlled fluid volumes. *Am. J. Physiol.* **247**, R537–R545 (1984).
42. D. B. Young, R. E. McCaa, Y. J. Pan and A. C. Guyton. Effectiveness of the aldosterone-sodium and potassium feedback control system. *Am. J. Physiol.* **231**, 945–953 (1976).
43. J. Diezi, P. Michoud, J. Aceves and G. Giebisch. Micropuncture study of electrolyte transport across papillary collecting duct of the rat. *Am. J. Physiol.* **224**, 623–634 (1973).
44. J. E. Hall, J. P. Granger, M. J. Smith, Jr. and A. J. Premen. Renal hemodynamics and arterial pressure in aldosterone escape. *Circ. Res.* **6**(Suppl. I), 1183–1192 (1984).
45. L. G. Navar and L. Rosivall. Contribution of the renin-angiotensin system to the control of intrarenal hemodynamics. *Kidney Int.* **25**, 857–868 (1984).
46. R. H. Fagard, A. W. Cowley, Jr., L. G. Navar, H. G. Langford and A. C. Guyton. Renal responses to slight elevations in renal arterial plasma angiotensin II concentration in dogs. *Clin. Exp. Pharmacol. Physiol.* **3**, 19–26 (1976).
47. D. W. Ploth and R. N. Roy. Renin-angiotensin influences on tubuloglomerular feedback activity in the rat. *Kidney Int.* **22**(Suppl. 2), S114–S121 (1982).
48. G. F. DiBona. The function of the renal nerves. *Rev. Physiol. Biochem. Pharmacol.* **94**, 76–181 (1982).
49. J. L. Osborn and R. J. Roman. Influence of low frequency renal nerve stimulation on renal sodium and bicarbonate excretion. *Fed. Proc.* **43**, 737 (1985).
50. J. L. Osborn, L. L. Francisco and G. F. DiBona. Effect of renal nerve stimulation on renal blood flow autoregulation and antinatriuresis during reduction in renal perfusion pressure. *Proc. Soc. Exp. Biol. Med.* **168**, 77–81 (1981).
51. D. W. Seldin and F. C. Rector. Evaluation of clearance methods for localization of the site of action of diuretics. In *Modern Diuretic Therapy in the Treatment of Cardiovascular and Renal Diseases* (Edited by L. F. Lant), pp. 97–110. Excepta Medica, Amsterdam (1973).
52. H. Valtin, *Renal Dysfunction*, pp. 227–313. Little, Brown and Company, Boston (1979).
53. N. G. Levinsky, E. A. Alexander and M. A. Venkatachalam. Acute renal failure. In *The Kidney* (Edited by B. M. Brenner and F. C. Rector), Vol. I, pp. 1181–1236. Saunders, Philadelphia (1981).
54. S. L. Linas and R. W. Schrier. The renin-angiotensin-aldosterone system and the etiology of hypertension in renal disease. In *The Kidney* (Edited by B. M. Brenner and F. C. Rector), Vol. II, pp. 2344–2379. Saunders, Philadelphia (1981).